Ultrahigh ionic conductivity in optimally sintered Li10.35Ge1.35P1.65S12 superionic conductor

Hao Wen
Sichuan University - Wangjiang Campus: Sichuan University
Yue Jiang
Sichuan University - Wangjiang Campus: Sichuan University
Xingang Liu
Sichuan University - Wangjiang Campus: Sichuan University
Xiaohong Zhu
Sichuan University - Wangjiang Campus: Sichuan University
Chuhong Zhang (chuhong.zhang@scu.edu.cn)
Sichuan University https://orcid.org/0000-0002-3378-7570

Nano Express

Keywords: lithium superionic conductor, sulfide, solid electrolyte, solid-state reaction, lithium ion battery.

DOI: https://doi.org/10.21203/rs.3.rs-79495/v1

Abstract

Lithium superionic conductor $Li_{10+\delta}Ge_{1+\delta}P_{2-\delta}S_{12}$ has attracted tremendous interest for advanced all-solid-state lithium ion batteries due to extremely high ionic conductivity. However, the synthetic processes reported in literature are widely divergent, resulting in an order of magnitude difference in ionic conductivities of the same material, but as far as we know, the influence of synthetic conditions on ionic conductivity has not been studied yet. Herein, we systematically investigate the influence of sintering temperature on phase composition and ionic conductivity of the $Li_{10+\delta}Ge_{1+\delta}P_{2-\delta}S_{12}$ compounds synthesized by conventional solid-state reaction for the first time. It is found that low and high sintering temperatures lead to a low crystallinity and the formation of impurity phases, respectively. As a result, the pure $Li_{10.35}Ge_{1.35}P_{1.65}S_{12}$, well crystallized in space group P42/nmc, is fabricated by optimization of the solid-state reaction temperature at 580 °C and its room temperature conductivity (19 mS cm^{-1}) is the highest among all existing $Li_{10+\delta}Ge_{1+\delta}P_{2-\delta}S_{12}$ solid electrolytes. Meanwhile, the microstructure of $Li_{10.35}Ge_{1.35}P_{1.65}S_{12}$, being very dense and uniform, is demonstrated firstly by atomic force microscopy.

Introduction

Lithium ion batteries (LIBs) have been used as power sources for a wide range of portable electric devices because of their high energy density, light weight and long cycle life.[1] However, the safety issues, which originate from combustible and leaky organic/liquid electrolytes, are of great concern with respect to vehicle or grid applications.[2] Solid-state electrolytes are escalating to prominence as useful components in advanced LIBs technologies due to their excellent electrochemical stability, favorable mechanical properties and feasible operation over a wide temperature window.[3–5] Nonetheless, one major obstacle in the application of solid-state electrolytes is that their ionic conductivities are lower than 1 mS cm^{-1} at room temperature.[6] In an effort to enhance the Li-ion conductivity, there have been relentless searches over the past few decades for new materials as solid electrolytes, such as crystalline (Li_3N, LIPON ($Li_xPO_yN_z$), LISICON ($Li_{14}ZnGe_4O_{16}$), NASICON ($Li_{1+x}Al_xTi_{2-x}(PO_4)_3$), perovskite-structured $Li_{3x}La_{2/3-x}TiO_3$ and garnet-structured $Li_7La_3Zr_2O_{12}$), glassy (Li_2S-P_2S_5, Li_2S-GeS_2, Li_2S-SiS_2) and polymer (PEO) systems.[7–14] Unfortunately, none of these materials possesses conductivities comparable to those of organic liquid electrolytes that are currently being used in commercial LIBs.

A big step towards solving this problem has been made until the discovery of $Li_{10}GeP_2S_{12}$ (LGPS) by Kanno et al. in 2011. The lithium ionic conductor LGPS with a different crystal structure from the thio-LISICON phase shows a very high ionic conductivity of 12 mS cm^{-1} at ambient temperature, which almost equals the conductivity value of 1 M $LiPF_6$ in the carbonate solvents.[15] It is generally believed that the high conductivity in LGPS is attributed to the fast diffusion of Li^+ in its crystal structure, which consists of PS_4 tetrahedra, $(Ge_{0.5}P_{0.5})S_4$ tetrahedra, LiS_6 octahedra and LiS_4 tetrahedra,[16–18] and more precisely, the 3D diffusion pathways along the *c* channel and along the *ab* plane as well.[19–21] The appearance of LGPS prompted enormous efforts to synthesize this material, and corresponding all-solid-

state batteries using this solid electrolyte were also fabricated and studied.[22–24] Nevertheless, the reported synthetic processes for LGPS are widely divergent, resulting in an order of magnitude change in ionic conductivities (1–12 mS cm^{-1}).[15,17,25–28] The difference of the conductivities may be caused by the varies synthetic conditions, such as calcination temperature or time, which play an crucial role to the final ionic conductivities of LGPS. However, this has not been elucidated in the published literature as far as we know. Meanwhile, it was recognized that a higher ionic conductivity can be obtained by adjusting the stoichiometric ratio of constructing elements in LGPS, i.e. the similar solid solution system $Li_{10+\delta}Ge_{1+\delta}P_{2-\delta}S_{12}$ ($0 \leq \delta \leq 0.5$). Up to now, the highest ionic conductivity of reported $Li_{10+\delta}Ge_{1+\delta}P_{2-\delta}S_{12}$ system is 14.2 mS cm^{-1} for $Li_{10.35}Ge_{1.35}P_{1.65}S_{12}$ ($\delta = 0.35$) at 27 ℃,[29] but no attempt has been made to further improve its ionic conductivity by changing the synthesis condition.

Therefore, in the present study, phase-pure $Li_{10.35}Ge_{1.35}P_{1.65}S_{12}$ was synthesized by a conventional solid-state reaction method in a sealed and evacuated quartz tube. The influences of sintering temperature on the phase composition, crystallinity, grain size and ionic conductivities were systematically studied. Upon process optimization, an ultrahigh ionic conductivity was achieved, reaching as high as 19 mS cm^{-1}.

Experimental Section

The starting materials used in this work were Li_2S (Aldrich, > 99.98% purity), GeS_2 (Leshan China, > 99.999% purity) and P_2S_5 (Aladdin, > 99% purity). These materials were weighed in an appropriate molar ratio, placed into a glass bottle and mixed for 30 min using a vibrating mill. All the starting materials were handled under a high purity argon atmosphere to prevent decomposition of the materials in reaction with external moisture and oxygen. The homogeneously mixed powders were then sealed in a quartz tube at 0.03 Pa (evacuated by a molecular pump, T-Station 75, Edwards) and sintered at various temperatures ranging from 550 to 600 °C in a step of 10 °C for 8 h in a furnace with 3 °C min^{-1} heating rate and 1 °C min^{-1} cooling rate. After that, the pre-synthesized material was ground to a fine powder using a mortar, pressed into pellets (about 6.5 mm in diameter and 0.9 mm in thickness) under 5 MPa pressure and sealed in a quartz tube again. In order to make the grains grow equally, the pellets were finally sintered at a certain temperature of 550 °C with the same heating and cooling rates as those used in powder sintering step.

Some of the sintered samples were ground to powders and sealed in quartz capillaries (about 0.7 mm in diameter) for X-ray diffraction (XRD) measurements, using an X-ray diffractometer under transmission mode (SmartLab3, Rigaku) with Cu Kα radiation (λ = 1.54056 Å). Diffraction data were collected at each 0.02° step width over the 2θ range from 10° to 60°. The surface morphology and grain size of the pellets were characterized by atomic force microscopy (AFM, Anasys AFM+). Meanwhile, some other pellets were sputtered with Au onto both sides of the pellets as electrodes by using an ion beam sputtering system (SBC-12, KYKY, Beijing) in an Ar-filled glove box for electrochemical impedance spectroscopy (EIS) measurements. This was performed with an Autolab PGSTAT302N system by applying an AC signal

with amplitude of 5 mV over the frequency range from 1 MHz to 1 Hz. The ionic conductivities were deduced from AC impedance results.

Results And Discussion

Figure 1 shows the XRD patterns of $Li_{10.35}Ge_{1.35}P_{1.65}S_{12}$ sintered at different temperatures in comparison to the computed result. The main phase of LGPS was observed in all these materials. Although the diffraction peaks of the 550 °C sintered sample completely coincide with the computed result, the peaks intensity is very weak, indicating poor crystallinity. As the sintering temperature is sequentially raised up to 580 °C, the diffraction peak intensity under exactly the same measurement conditions becomes gradually stronger and thus the 580 °C sample shows the best crystallinity. However, with a further increase in the sintering temperature to 590 and 600 °C, the crystallinity starts to degrade. Furthermore, other phases are noticeable in the XRD patterns and are distinctly different from those obtained in the samples sintered below 580 °C, which are confirmed to match well with γ-Li_3PS_4 and GeS_2 via the JADE program and are marked as hollow triangle (∇) and hollow box (□) in Fig. 1, respectively. It can be seen from the figure that the peak intensity of these impurity phases becomes stronger when the sintering temperature increases from 590 to 600 °C, revealing that heat treatment of $Li_{10.35}Ge_{1.35}P_{1.65}S_{12}$ at high temperatures above 580 °C would lead to the formation of impurity phases like γ-Li_3PS_4 and GeS_2. Therefore, it is determined that the most suitable sintering temperature is 580 °C for the synthesis of $Li_{10.35}Ge_{1.35}P_{1.65}S_{12}$. A lower sintering temperature would result in lower crystallinity, while a higher sintering temperature would lead to the formation of impurity phases.

The structural profile parameters of $Li_{10.35}Ge_{1.35}P_{1.65}S_{12}$ sintered at 580 °C were refined by Rietveld analysis with the refinement program FullProf. Figure 2 and Table 1 provide the Rietveld refinement pattern and results. The space group P42/nmc is verified and the unit cell parameters obtained in our present work (a = 8.7002 Å, c = 12.6274 Å) are similar to those reported in the literature.[15–18]

Table 1
Rietveld refinement results for $Li_{10.35}Ge_{1.35}P_{1.65}S_{12}$ sintered at 580 °C.

Atom	Site	*x*	*y*	*z*
Li1	14 h	0.24593	0.27197	0.19500
Li2	4d	0	1/2	0.94434
Li3	8f	0.23543	= *x*(Li3)	0
Li4	4c	0	0	0.26841
Ge1	4d	0	1/2	0.69126
P1	4d	0	1/2	0.69126
P2	2b	0	0	1/2
S1	8 g	0	0.18862	0.40801
S2	8 g	0	0.29416	0.09556
S3	8 g	0	0.70168	0.79410
Note: Space group $P4_2/nmc$ (137), a = 8.7002(3) Å, c = 12.6274(5) Å, V = 955.8119 Å^3, R_p=14.2, R_{wp}=14.9, R_{exp}=11.5, R_B=2.9, R_F=2.6.				

AFM analysis was used here for characterization of $Li_{10.35}Ge_{1.35}P_{1.65}S_{12}$'s microstructure and grain size. Figure 3 shows the two-dimensional AFM micrographs of $Li_{10.35}Ge_{1.35}P_{1.65}S_{12}$ sintered at 550, 580 and 600 °C, respectively. For each AFM image, the area in view represents a 10 μm × 10 μm square. The roughly estimated grain size of 550 °C sintered sample is about 1–2 μm. As shown in the figure, with an increase in sintering temperature, the grain size increases gradually, and thus, a positive correlation between grain size and sintering temperature is obtained in $Li_{10.35}Ge_{1.35}P_{1.65}S_{12}$, like what was generally observed in many other inorganic materials. The most uniform and dense microstructure is, however, achieved in the 580 °C sintered sample.

Figure 4 presents the room-temperature impedance spectra for the samples sintered at different temperatures and the high frequency parts are magnified in the inset. Similar to the widely reported results for sulfide electrolytes, these plots only exhibit an oblique line in the frequency range of 1 MHz to 1 Hz, and similarly, the horizontal intercept of oblique lines presented in Fig. 4 can be identified as the total resistance R of samples. Accordingly, the ionic conductivity is calculated as $\sigma = L/(R \times A)$, where L and A are the thickness and area of the pellets, respectively.[30]

Figure 5 illustrates the calculated room-temperature conductivities as a function of the sintering temperature. As shown in this figure, the conductivity increases first and then decreases with the increase

in sintering temperature. When the sintering temperature is 550 °C, the obtained conductivity is 13.8 mS cm^{-1}, and is close to the previously reported result.[29] Very interestingly, the highest ionic conductivity, obtained in the 580 °C sample, reaches as high as 19 mS cm^{-1}. This is the highest lithium-ion conductivity obtained experimentally at room temperature for $Li_{10+\delta}Ge_{1+\delta}P_{2-\delta}S_{12}$, to the best of our knowledge. However, when the sintering temperature exceeds 580 °C, the ionic conductivity decreases sharply. For example, the conductivity of the sintered sample at 600 °C (10.2 mS cm^{-1}) is just 53.7% of the value of the 580 °C sintered one. Taking the XRD patterns into account, the crystallinity of samples peaks as the sintering temperature rises up to 580 °C. Moreover, the grain size of these samples increases with increasing the sintering temperature, as previously presented in Fig. 3. Accordingly, the total superficial area of grains does change in the same way as grain size and the Li^+ migration distance among $Li_{10.35}Ge_{1.35}P_{1.65}S_{12}$ grains changes as well, and therefore, the ionic conductivity is enhanced. Besides, the γ-Li_3PS_4 phase, with a low ionic conductivity on the order of 10^{-4} mS cm^{-1},[31] forms in the high temperature region, which attributes to the sharp decrease of the overall conductivity. With the highest ionic conductivity as well as the best crystallinity and microstructure, it is concluded that 580 °C is the best sintering temperature for $Li_{10.35}Ge_{1.35}P_{1.65}S_{12}$.

Conclusions

In this study, the LGPS-type solid electrolytes $Li_{10.35}Ge_{1.35}P_{1.65}S_{12}$ with high ionic conductivities have been synthesized at different sintering temperature by solid-state reaction. Either low crystallinity or phase impurity features below and above 580 ℃, respectively, both leading to a sharp decrease in ionic conductivity. As a result, an ultrahigh ionic conductivity of 19 mS cm^{-1} is achieved for the 580 ℃ sintered sample, which is the highest values for all $Li_{10+\delta}Ge_{1+\delta}P_{2-\delta}S_{12}$ solid electrolytes reported so far.

Abbreviations

LGPS: $Li_{10}GeP_2S_{12}$; PEO: polyethylene oxide

Declarations

Acknowledgements

This work was financially supported by the Ministry of Science and Technology of China (MOST) (973 program, No. 2013CB934700) and the National Natural Science Foundation of China (Nos. 51222305 and 51673123).

Authors' contributions

Hao Wen and Yue Jiang contributed equally to this study. The authors read and approved the final manuscript.

Availability of data and materials

All data are fully available without restriction.

Competing interests

The authors declare that they have no competing interests.

References

1. Goodenough JB, Kim Y (2010) Challenges for rechargeable Li batteries. Chem. Mater. 22(3):587-603.
2. Biensan P, Simon B, Peres JP, Guibert AD, Broussely M, Bodet JM, Perton F (1999) On safety of lithium-ion cells. J. Power Sources 81:906-912.
3. Fergus JW (2010) Ceramic and polymeric solid electrolytes for lithium-ion batteries. J. Power Sources 195(15):4554-4569.
4. Aravindan V, Gnanaraj J, Madhavi S, Liu HK (2011) Lithium-ion conducting electrolyte salts for lithium batteries. Chem.-Eur. J. 17(51):14326-14346.
5. Knauth P (2009) Inorganic solid Li ion conductors: An overview. Solid State Ionics 180(14-16):911-916.
6. Takada K (2013) Progress and prospective of solid-state lithium batteries. Acta Mater. 61(3):759-770.
7. Stramare S, Thangadurai V, Weppner W (2003) Lithium lanthanum titanates: A review. Chem. Mater. 15(21):3974-3990.
8. Murugan R, Thangadurai V, Weppner W (2007) Fast lithium ion conduction in garnet-type $Li_7La_3Zr_2O_{12}$. Angew. Chem. Int. Ed. 46(41):7778-7781.
9. Kanno R, Murayama M (2001) Lithium ionic conductor thio-LISICON: The Li_2S-GeS_2-P_2S_5 J. Electrochem. Soc. 148(7):A742-A746.
10. Hayashi A, Tatsumisago M (2012) Recent development of bulk-type solid-state rechargeable lithium batteries with sulfide glass-ceramic electrolytes. Electron. Mater. Lett. 8(2):199-207.
11. Noto VD, Lavina S, Giffin GA, Negro E, Scrosati B (2011) Polymer electrolytes: Present, past and future. Eletrochim. Acta 57:4-13.
12. Mizuno F, Hayashi A, Tadanaga K, Tatsumisago M (2005) New, highly ion-conductive crystals precipitated from Li_2S-P_2S_5 Adv. Mater. 17(7):918-921.
13. Aldissi M (2001) Multi-layered polymer electrolytes towards interfacial stability in lithium ion batteries. J. Power Sources 94(2):219-224.
14. Adachi GY, Imanaka N, Aono H (1996) Fast Li^+ conducting ceramic electrolytes. Adv. Mater. 8(2):127-135.

15. Kayama N, Homma K, Yamakawa Y, Hirayama M, Kanno R, Yonemura M, Kamiyama T, Kato Y, Hama S, Kawamoto K, Mitsui A (2011) A lithium superionic conductor. Nat. Mater. 10:682-686.
16. Ong SP, Richards WD, Miara L, Lee HS, Ceder G (2013) Phase stability, electrochemical stability and ionic conductivity of the $Li_{10\pm1}MP_2X_{12}$ (M = Ge, Si, Sn, Al or P, and X = O, S or Se) family of superionic conductors. Energy Environ. Sci. 6(1):148-156.
17. Hassoun J, Verrelli R, Reale P, Panero S, Mariotto G, Greenbaum S, Scrosati B (2013) A structural, spectroscopic and electrochemical study of a lithium ion conducting $Li_{10}GeP_2S_{12}$ solid electrolyte. J. Power Sources 229:117-122.
18. Hori S, Suzuki K, Hirayama M, Kato Y, Saito T, Yonemura M, Kanno R (2014) Synthesis, structure, and ionic conductivity of solid solution, $Li_{10+\delta}M_{1+\delta}P_{2-\delta}S_{12}$ (M = Si, Sn). Faraday Disscuss. 176:83-94.
19. Weber DA, Senyshyn A, Weldert KS, Wenzel S, Zhang WB, Kaiser R, Berendts S, Janek J, Zeier WG (2016) Structural insights and 3D diffusion pathway within the lithium superionic conductor $Li_{10}GeP_2S_{12}$. Chem. Mater. 28(16):3974-3990.
20. Bhandari A, Bhattacharya J (2016) Origin of fast ion conduction in $Li_{10}GeP_2S_{12}$, a superionic conductor. J. Phys. Chem. C 120(51):29002-29010.
21. Sang LZ, Haasch RT, Gewirth AA, Nuzzo RG (2017) Evolution at the solid electrolyte/gold electrode interface during lithium deposition and stripping. Chem. Mater. 29(7):3029-3037.
22. Yin JY, Yao XY, Peng G, Yang J, Huang Z, Liu D, Tao YC, Xu XX (2015) Influence of the Li-Ge-P-S based solid electrolytes on NCA electrochemical performances in all-solid-state lithium batteries. Solid State Ionics 274:8-11.
23. Zhang Q, Peng G, Mwizerwa JP, Wan HL, Cai LT, Xu XX, Yao XY (2018) Nickel sulfide anchored carbon nanotubes for all-solid-state lithium batteries with enhanced rate capability and cycling stability. J. Mater. Chem. A 6(25):12098-12105.
24. Cai LT, Zhang Q, Mwizerwa JP, Wan HL, Yang XL, Xu XX, Yao XY (2018) Highly crystalline layered VS_2 nanosheets for all-solid-state lithium batteries with enhanced electrochemical performances. ACS Appl. Mater. Interfaces 10(12):10053-10063.
25. Kuhn A, Duppel V, Lotsch BV (2013) Tetragonal $Li_{10}GeP_2S_{12}$ and Li_7GePS_8 – exploring the Li ion dynamics in LGPS Li electrolytes. Energy Environ. Sci. 6(12):3548-3552.
26. Han FD, Gao T, Zhu YJ, Gaskell KJ, Wang CS (2015) A battery made from a single material. Adv. Mater. 27(23):3473-3483.
27. Sun Y, Yan WN, An L, Wu BB, Zhong KF, Yang RZ (2017) A facile strategy to improve the electrochemical stability of a lithium ion conducting $Li_{10}GeP_2S_{12}$ solid electrolyte. Solid State Ionics 301:59-63.
28. Zhang H, Li XH, Hao SM, Zhang X, Lin JP (2019) Inducing interfacial progress based on a new sulfide-based composite electrolyte for all-solid-state lithium batteries. Eletrochim. Acta 325:134943.
29. Kwon O, Hirayama M, Suzuki K, Kato Y, Saito T, Yonemura M, Kamiyama T, Kanno R (2015) Synthesis, structure, and conduction mechanism of the lithium superionic conductor $Li_{10+\delta}Ge_{1+\delta}P_{2-}$

$_{\delta}S_{12}$. J. Mater. Chem. A 3(1):438-446.

30. Chandra A, Bhatt A, Chandra A (2013) Ion conduction in superionic glassy electrolytes: An overview. J. Mater. Sci. Technol. 29(3):193–

31. Homma K, Yonemura M, Kobayashi T, Nagao M, Hirayama M, Kanno R (2011) Crystal structure and phase transitions of the lithium ionic conductor Li_3PS_4. Solid State Ionics 182(1):53–

Figures

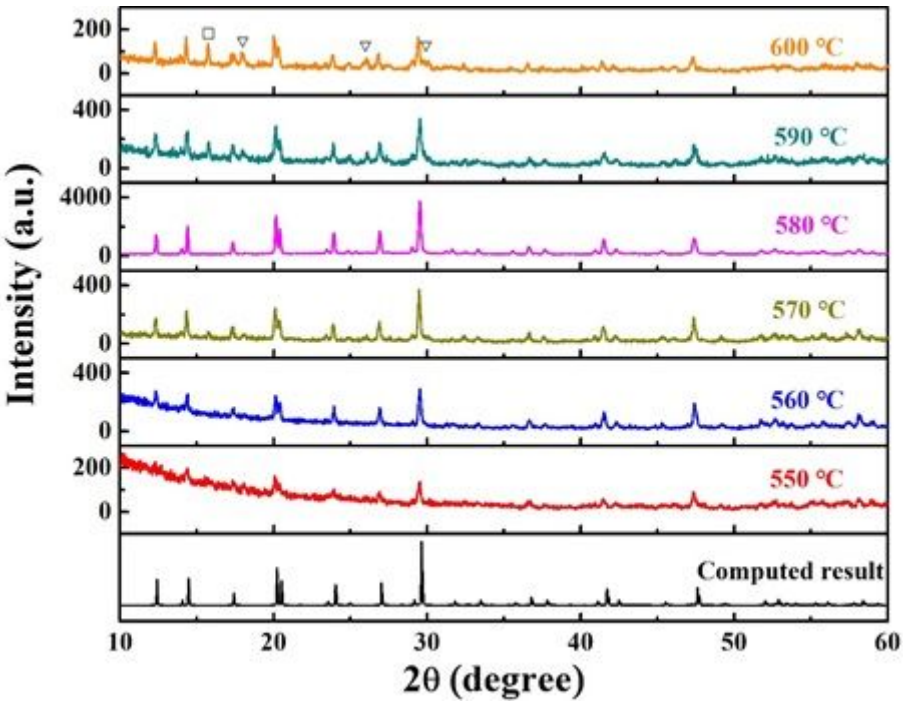

Figure 1

X-ray diffraction patterns for Li10.35Ge1.35P1.65S12 sintered at different temperatures (550, 560, 570, 580, 590 and 600 °C) in comparison with the computed result. The γ-Li3PS4 and GeS2 impurity phases are marked with hollow triangle (▽) and hollow box (□), respectively.

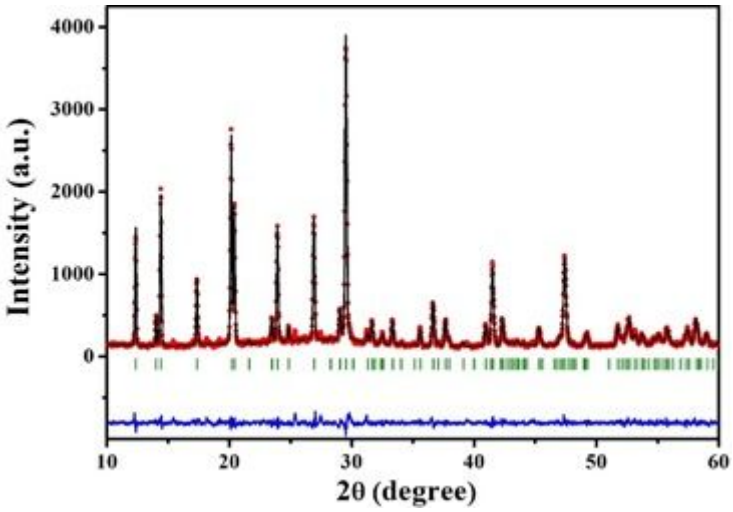

Figure 2

X-ray Rietveld refinement pattern for Li10.35Ge1.35P1.65S12 sintered at 580 °C. Observed data (red dots), calculated pattern (black line), and the difference between the two (blue line) are shown. Green vertical bars indicate the positions of Bragg reflections.

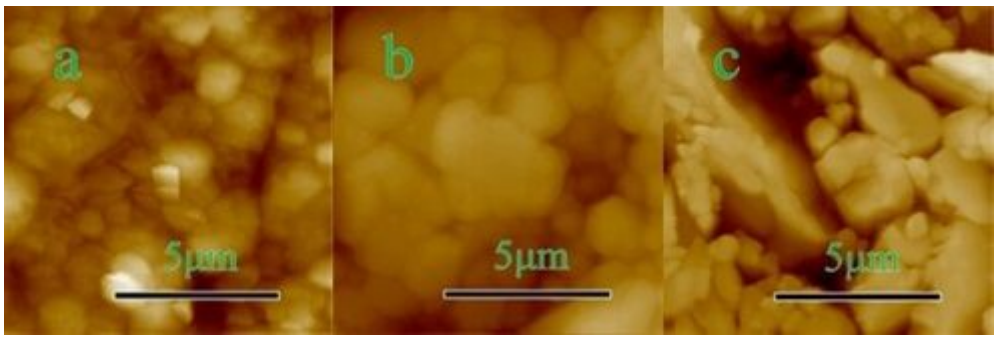

Figure 3

Two dimensional AFM micrographs of Li10.35Ge1.35P1.65S12 sintered at (a) 550 °C, (b) 580 °C and (c) 600 °C.

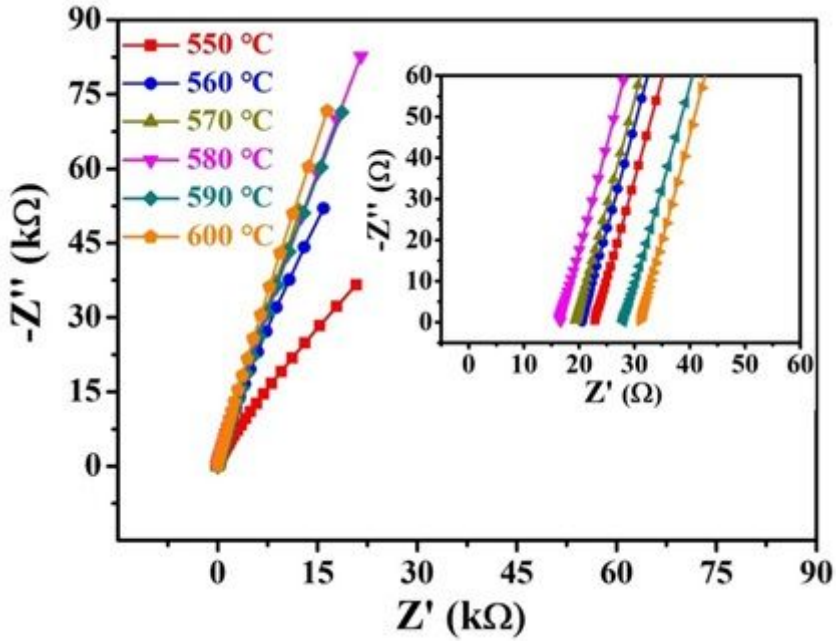

Figure 4

Room-temperature impedance spectra for the samples sintered at different temperatures. The high frequency parts are magnified in the inset.

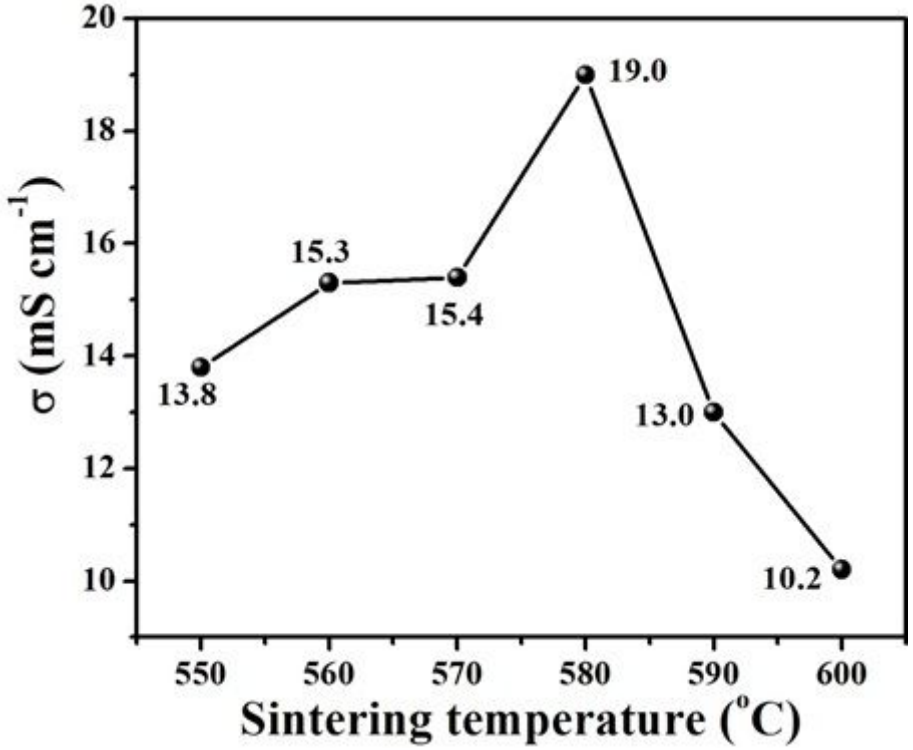

Figure 5

Calculated conductivities at room temperature as a function of the sintering temperature for the Li10.35Ge1.35P1.65S12 samples.